Check for updates

ADVANCED MATERIALS
www.advmat.de

Ring-Opening Polymerization of Surface Ligands Enables Versatile Optical Patterning and Form Factor Flexibility in Quantum Dot Assemblies

Yunseo Lee, Jiyun Shin, Seungki Shin, Eun A Kim, Joon Yup Lee, Namyoung Gwak, Seongchan Kim, Jaeyoung Seo, Hyein Kong, Dongjoon Yeo, Jina Na, Sungwon Kim, Juho Lee, Seong-Yong Cho, Jaejun Lee, Tae Ann Kim,* and Nuri Oh**

The evolution of display technologies is rapidly transitioning from traditional screens to advanced augmented reality (AR)/virtual reality (VR) and wearable devices, where quantum dots (QDs) serve as crucial pure-color emitters. While solution processing efficiently forms QD solids, challenges emerge in subsequent stages, such as layer deposition, etching, and solvent immersion. These issues become especially pronounced when developing diverse form factors, necessitating innovative patterning methods that are both reversible and sustainable. Herein, a novel approach utilizing lipoic acid (LA) as a ligand is presented, featuring a carboxylic acid group for QD surface attachment and a reversible disulfide ring structure. Upon i-line UV exposure, the LA ligand initiates ring-opening polymerization (ROP), crosslinking the QDs and enhances their solvent resistance. This method enables precise full-color QD patterns with feature sizes as small as 3 µm and pixel densities exceeding 3788 ppi. Additionally, it supports the fabrication of stretchable QD composites using LA-derived monomers. The reversible ROP process allows for flexibility, self-healing, and QD recovery, promoting sustainability and expanding QD applications for ultra-fine patterning and on-silicon displays.

1. Introduction

The demand for ultrahigh-resolution patterning in display technology has surged with the rise of immersive experiences like augmented reality (AR) and virtual reality (VR). Colloidal quantum dots (QDs) are at the forefront of this technological shift due to their tunable optical properties, governed by their core size and the varied compositions of their shell and surface ligands. These characteristics make QDs ideal for applications in LEDs, detectors, and solar cells.[1–3] However, to fully harness these advantages in solution-processed manufacturing, the precise placement of QDs in designated locations is essential. Conventional QD patterning techniques, such as transfer printing,[4–6] inkjet printing,[7,8] and photolithography,[9–13] have been developed to address this requirement, but they present significant challenges. These

Y. Lee, S. Shin, N. Gwak, S. Kim, J. Seo, H. Kong, D. Yeo, J. Na, S. Kim, N. Oh
Division of Materials Science and Engineering
Hanyang University
Seoul 04763, Republic of Korea
E-mail: irunho@hanyang.ac.kr

J. Shin, J. Lee, T. A. Kim
Solutions to Electromagnetic Interference in Future-mobility Research Center
Korea Institute of Science and Technology
Seoul 02792, Republic of Korea
E-mail: takim717@kist.re.kr

The ORCID identification number(s) for the author(s) of this article can be found under https://doi.org/10.1002/adma.202415436

© 2025 The Author(s). Advanced Materials published by Wiley-VCH GmbH. This is an open access article under the terms of the Creative Commons Attribution-NonCommercial-NoDerivs License, which permits use and distribution in any medium, provided the original work is properly cited, the use is non-commercial and no modifications or adaptations are made.

[Correction added on January 17, 2025, after first online publication: Affiliations of Juho Lee and Joon Yup Lee has been updated.]

DOI: 10.1002/adma.202415436

E. A Kim, J. Y. Lee, S.-Y. Cho
Department of Photonics and Nanoelectronics
BK21 FOUR ERICA-ACE Center
Hanyang University ERICA
Ansan 15588, Republic of Korea

J. Lee, T. A. Kim
Division of Energy & Environment Technology
KIST School
Korea University of Science and Technology (UST)
Seoul 02792, Republic of Korea

J. Lee
Department of Polymer Science and Engineering
Pusan National University
Busan 46241, Republic of Korea
E-mail: jlee-pse@pusan.ac.kr

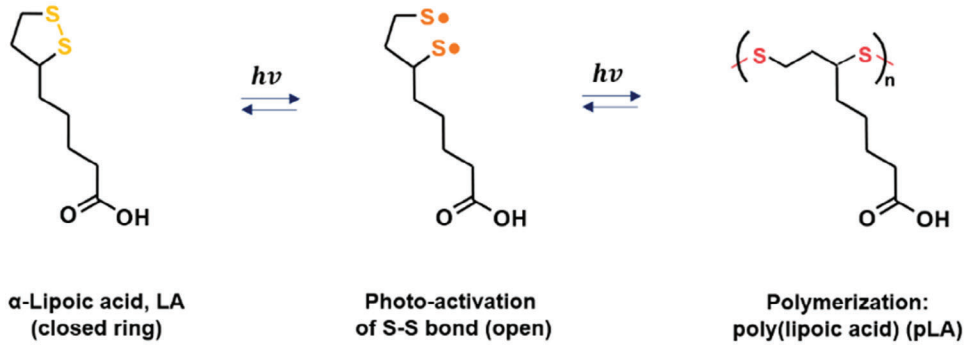

Scheme 1. Molecular structure and schematic of the ROP of LA under UV irradiation.

methods often suffer from reactivity with surface ligands and poor solvent resistance.[13,14] Conventional photolithography can cause decreased photoluminescence (PL) due to interactions with photoresists and solvents. Such limitations hinder the scalability and overall performance of QD-based devices.

To overcome these challenges, direct optical patterning of QD solids has emerged as a promising alternative.[15] This technique involves selectively exposing areas to UV light, which induces differential solubility. The UV-exposed regions resist dissolution by solvents, thereby enabling precise QD patterning. To achieve this, various ligands have been proposed to control the solubility of QD assemblies. One effective approach uses photoactive ligands, such as photoacid and photobase generators, which undergo chemical transformations upon UV exposure.[16,17] These optically activated ligands passivate surface defects on QDs, preventing aggregation and enabling controlled solubility modulation. However, despite these advantages, unresolved issues, such as PL degradation, persist. Another approach involves ligand decomposition, where a stimulus causes the ligand to break down into fragments, altering the charge and polarity on the QD surface.[18–20] While effective, this method involves complex procedures that are difficult to implement.

Alternative strategies have been proposed to mitigate PL degradation and streamline the QD patterning process. One strategy is the addition of small amounts of additives to crosslinking ligands to facilitate pattern formation,[9,10,12] which has been successfully applied in light-emitting devices. However, challenges like QD aggregation and precise UV exposure time still pose difficulties. Another approach explores patterning through ligand substitution using a dual-ligand configuration, achieving high resolution[9] but introducing complexities due to intricate procedures and bulky ligands. Consequently, a comprehensive understanding of these methodologies is crucial for advancing high-resolution QD patterning for pixelated optoelectronic devices.

In this paper, we propose an innovative QD assembly and patterning technique using lipoic acid (LA) as a polymerizable ligand. LA, a naturally occurring five-membered cyclic disulfide (1,2-dithiolane) with a carboxylic acid group, dissociates into diradicals under UV light, initiating radical ring-opening polymerization (ROP) (**Scheme 1** and Figure S1).[21,22] The dynamic nature of polymerization and depolymerization, driven by intermediate ring strain, makes LA an excellent candidate for QD crosslinking and patterning. Previous studies have focused on LA's dithiolane group as a multidentate ligand for robust interactions with QD surfaces.[23–27] In contrast, our approach leverages LA's ability to initiate outward polymerization[28] rather than just surface attachment. By introducing LA into the QD solution and exchanging a portion of the native ligands, UV exposure triggers the opening of LA's disulfide ring, leading to polymerization with other LA molecules. The UV-triggered reaction results in a network through sequential linear polymerization, simplifying the patterning process. Using this method, we successfully fabricated RGB multi-patterns with a minimum feature size of 3 μm and a high pixel density of 3788 pixels per inch (ppi). Additionally, we fabricated stretchable QD-polymer films by incorporating additional LA-derived monomers and crosslinkers. The enhanced ROP of LA derivatives throughout the medium produced free-standing and elastic composite materials. The reversible nature of cyclic disulfides allows for complete degradation of the network back into monomers, promoting sustainability in materials chemistry. These findings reveal the significant potential of diverse form-factor displays, including AR/VR technologies.

2. Results and Discussion

For the practical application of QDs, capping ligands should be both processable and suitable for environmentally friendly conditions. It is also desirable to enhance the optical properties of QDs, as patterning processes, such as solvent rinsing and UV exposure, may damage the delicate QD surfaces. Polymeric ligands offer advantages in QD ligand selection to meet these requirements.[29,30] LA was selected as an additive QD ligand due to its practicality in reversible ring-opening and closing reactions of cyclic disulfides (Scheme 1).

First, we introduced LA into the InP QD solution as a minor additive to aid in forming QD films. We anticipated that the carboxylic acid group in the LA molecule would effectively attach to the QD surface when the dithiolane group was in its closed state. Depending on the amount of LA added, some of the native surface ligands would be replaced. As shown in **Figure 1**, the native ligands on the surface, oleic acid, and metal oleates were proportionally exchanged with LA based on the amount added. Partial exchange of native ligands with LA resulted in negligible differences in colloidal stability and dispersion (Figure 1a). However, complete replacement with LA caused significant aggregation and reduced colloidal stability, as evidenced by the cloudy appearance of the solution and decreased spacing between the QDs in the TEM images.[29,31]

© 2025 The Author(s). Advanced Materials published by Wiley-VCH GmbH

15214095, 2025, 9, Downloaded from https://advanced.onlinelibrary.wiley.com/doi/10.1002/adma.202415436 by Korea Institute Of Science, Wiley Online Library on [24/07/2025]. See the Terms and Conditions (https://onlinelibrary.wiley.com/terms-and-conditions) on Wiley Online Library for rules of use; OA articles are governed by the applicable Creative Commons License

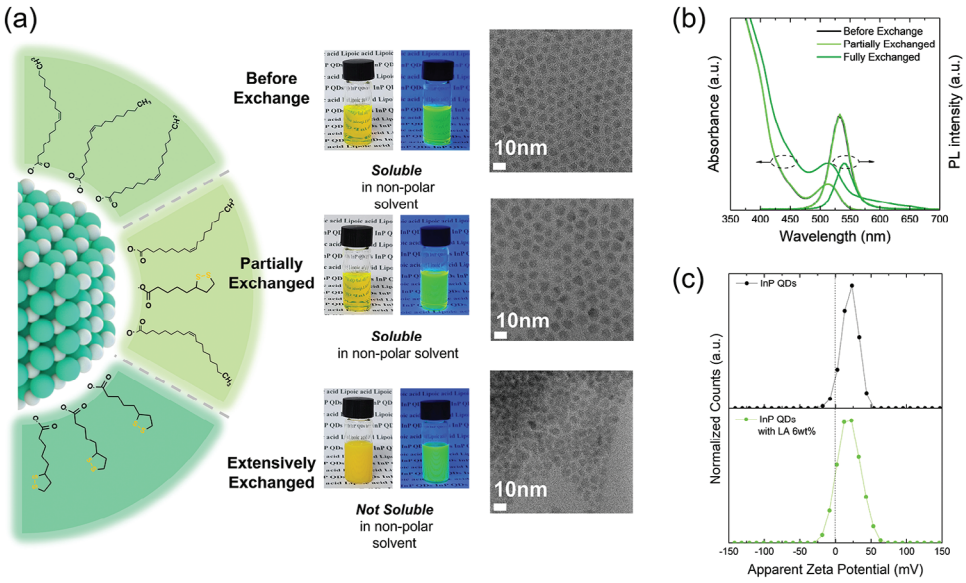

Figure 1. Ligand exchange process between LA and oleic acid-capped QDs. a) Schematic representation of ligand exchange process in InP QDs solution, Images of InP QDs solutions based on ligand contents (left image taken under room light, and right image taken under UV light) along with TEM images. b) Absorption and PL spectra of the InP QDs solutions with LA content. c) Zeta potentials of InP QDs solutions with oleic acid which is the native ligand and InP QDs containing LA.

Grazing incidence small-angle X-ray scattering (GISAXS) measurements were conducted to further evaluate the colloidal stability of the QD films with native or LA ligands (Figure S2). The results indicated that the interdot distance decreased from 8.35 nm for QDs with native ligands to 8.08 nm for QDs extensively exchanged with LA ligands. Consequently, the GISAXS pattern indicates reduced interparticle spacing between InP QDs due to the extensively exchanged LA ligands, resulting in a less uniform particle alignment and reduced film stability.[32,33] Additional insights into the effects of LA on QDs were obtained through TEM imaging. Figures S3 display TEM images of QDs capped with native ligands, partially exchanged LA, and extensively exchanged LA at different scales. The large clusters observed in Figures S3b, S3c, presumably polymerized LA, represent excess LA remaining after ligand exchange, with the cluster size increasing from partial to full exchange, indicating higher quantities of LA.[34] Importantly, the interplanar distance of the QDs remained unchanged, suggesting that LA did not affect the QDs themselves but crosslinked with surrounding LA. This will be discussed in more detail in the following sections.

As shown in Figure 1b, we examined the effect of LA ligand concentration on the optical properties of the QDs. The full exchange of native ligands with LA led to QD aggregation and changes in the optical properties. In contrast, partial exchange with LA maintained optical characteristics similar to those of the native ligands. The PL spectra revealed a redshift for extensively LA-exchanged QDs, while the partially LA-exchanged QDs did not exhibit significant changes. Time-resolved PL (TRPL) spectroscopy further showed that the average lifetime (τ_{avg}) of QDs with native ligands and those partially exchanged with LA were comparable, at 34.19 ns and 36.56 ns, respectively (Figure S4). However, QDs extensively exchanged with LA exhibited a sharply decreased τ_{avg} of 18.91 ns, attributed to exciton energy transfer between closely aggregated QDs.[35,36]

To confirm the successful partial ligand exchange of LA on the QD surface, replacing oleic acid and metal oleates, we measured the zeta potential after the addition of LA (Figure 1c). The positive zeta potential values indicated that the carboxyl groups of LA were well attached to the QD surface, confirming successful ligand exchange.[37] Previous studies have reported an alternative approach in which LA is introduced and UV light is used to open disulfide rings, allowing sulfur to attach to the QD surface.[25,26] If this method were applied to our QDs, the outward-oriented carboxyl groups would result in a negative zeta potential.[37] In contrast, our study proceeded without UV irradiation, ensuring that the disulfide rings remained closed. This resulted in positive zeta potential values because the carboxyl groups of LA adhered effectively to the QD surface. The partial ligand exchange in the QD solution allowed the carboxyl groups of LA to attach to the QD surface while the dithiolane groups were oriented outward, facilitating crosslinking between dithiolane groups in the QD films. The FTIR results presented in Figure S5 further support this, showing the emergence of distinct bands around 1700 cm^{-1} and 1650 cm^{-1}, which correspond to the chemical changes associated with LA coordination to InP QDs. This confirms that LA effectively replaces oleic acid as a ligand for InP QDs. The COO^- groups on QD surfaces enable dynamic coordination and ligand exchange, a process facilitated by the weak binding strength of oleic acid.[38] The carboxyl group in LA similarly coordinates to the QD surface, with its shorter molecular structure offering reduced steric hindrance and a greater propensity for ligand exchange compared to oleic acid. Supporting this, molecules containing both carboxyl groups and sulfur-based functionalities have been shown to bind dynamically to QD surfaces, further validating LA's suitability as a ligand.[15] Hereafter, we refer to these modified QDs as LA-InP QDs.

Partial LA ligand exchange enabled the formation of a stable QD network with enhanced solvent resistance. **Figure** 2a

© 2025 The Author(s). Advanced Materials published by Wiley-VCH GmbH

15214095, 2025, 9, Downloaded from https://advanced.onlinelibrary.wiley.com/doi/10.1002/adma.202415436 by Korea Institute Of Science, Wiley Online Library on [24/07/2025]. See the Terms and Conditions (https://onlinelibrary.wiley.com/terms-and-conditions) on Wiley Online Library for rules of use; OA articles are governed by the applicable Creative Commons License

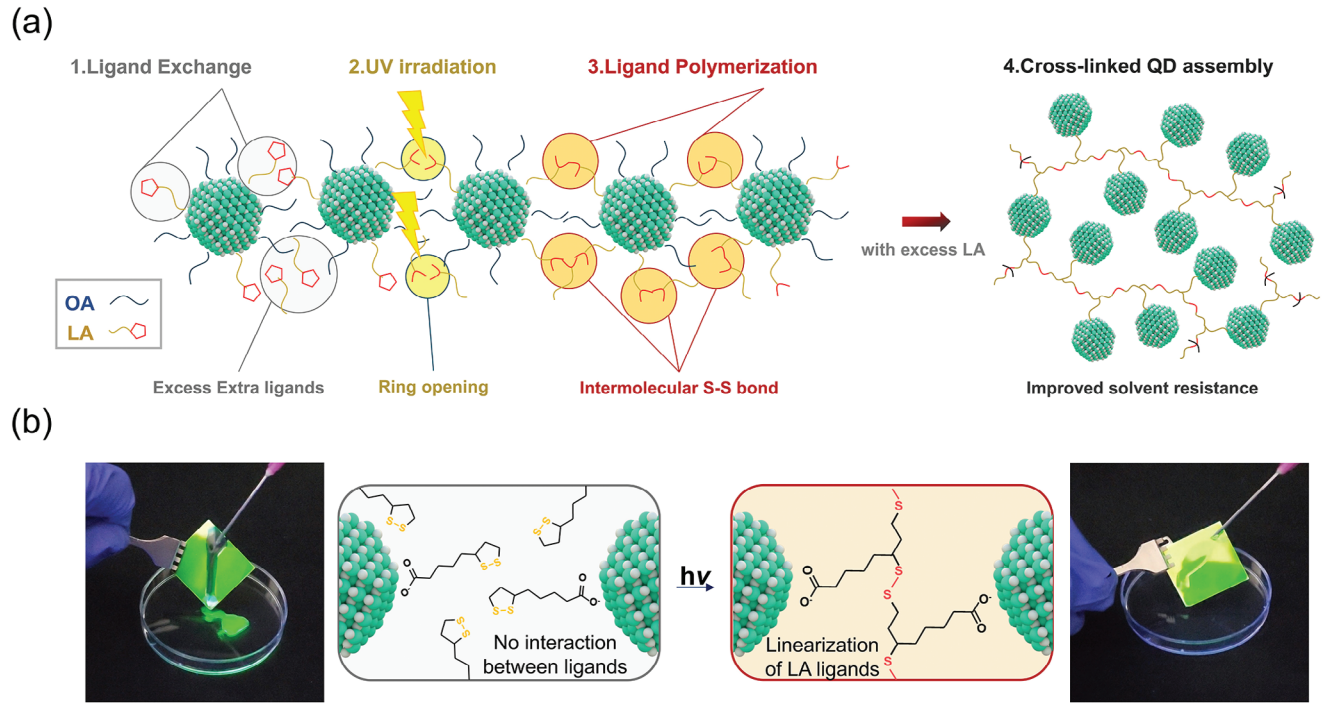

Figure 2. Lipoic acid assisted formation of QD assembly. a) Schematic of QD assembly through ROP after partial ligand exchange of InP QDs. b) Images of InP QDs films before and after ROP when toluene was dripped onto them.

illustrates the process of forming a QD network using LA-InP QDs. Upon UV irradiation, as described in Scheme 1, the disulfide ring of LA opens, initiating polymerization through the formation of S-S bonds with 1,2-dithiolanes from other LA ligands. The LA ligands adhered effectively to the QD surface due to the presence of carboxyl groups, as shown in Figure 1. The LA ligands on the QDs undergo ROP, with the QD particles acting as crosslinkers. As a result, the assembled QD film polymerized with LA ligands exhibited altered solubility in solvents.

Figure 2b shows images of the LA-InP QD films before and after UV irradiation, demonstrating the flow of the mother solvent, toluene. Before UV exposure, the disulfide rings of LA remained closed, allowing the thin-film form of the QDs to immediately dissolve in toluene. However, after UV exposure, the opened disulfide rings of LA initiated a sequential ROP, forming a polymerized QD network. During the ROP process, which utilizes LA as the ligand for InP QDs, no aggregation or morphological changes were observed among the QDs as shown in Figure S6. When toluene was flowed over the UV-irradiated QD film, the QDs remained intact without dissolution, indicating the successful formation of the QD network. To quantitatively evaluate the solvent resistance imparted by ROP, we analyzed the PL and absorbance spectra, as shown in Figure S7. Before ROP, the InP QDs films dissolved significantly upon toluene rinsing, leading to a pronounced reduction in PL intensity (Figures S7a, S7b). In contrast, after ROP, the PL intensity exhibited only a slight decrease, likely due to minor surface effects caused by exposure to solvent, air, or moisture. The absorbance spectra, however, showed no significant changes, confirming that the QD network remained intact (Figures S7c, S7d). These results further support the concept that stable QD patterns can be achieved through selective UV irradiation facilitated by LA ligand exchange in QDs.[25]

The formation of the QD-LA network was independent of the type of native ligands in the QDs. Figure S8 shows photographs of InP QD films with dodecane thiol and myristic acid ligands, where the ligands were partially exchanged with LA both before and after exposure to UV light and dipping in toluene. In both cases, ROP did not occur before UV irradiation, resulting in the dissolution of all QDs in the film when exposed to toluene. However, after UV irradiation, ROP occurred, altering the solubility in the solvent, as demonstrated by the fact that the QDs remained intact in toluene. Figure S7a confirms that when the ligands are dodecane thiol and LA, ROP occurs, indicating that the carboxylic acid group of LA attaches to the QD surface rather than the disulfide ring. Similarly, Figure S8b shows that when the ligands were LA and myristic acid, which lacks a double bond unlike oleic acid, ROP still occurred. This confirms that polymerization proceeds via the ring-opening reaction of LA rather than the addition of sulfur radicals to unsaturated carbon bonds.[12] In both cases, the change in solubility of the QD films indicates that LA attaches to the QD surface and facilitates the ROP of 1,2-dithiolane upon UV irradiation, resulting in altered solubility.

The conversion of LA to polymers was analyzed by ^{1}H NMR spectroscopy of the LA solution before UV exposure and the polymerized LA and pLA-InP QDs after UV light exposure (**Figure 3a**). Upon ROP of LA, the peaks from the methylene protons (a) and methine proton (c) adjacent to the sulfur atoms shifted and broadened ($a' + c'$), indicating a reduction in chemical bond tension within the disulfide ring.[28] The monomer conversion was determined by analyzing the peak integrals at $a' + c'$ (C-S-S-C protons from the polymer) and b_1 (one of the methylene

© 2025 The Author(s). Advanced Materials published by Wiley-VCH GmbH

15214095, 2025, 9, Downloaded from https://advanced.onlinelibrary.wiley.com/doi/10.1002/adma.202415436 by Korea Institute Of Science, Wiley Online Library on [24/07/2025]. See the Terms and Conditions (https://onlinelibrary.wiley.com/terms-and-conditions) on Wiley Online Library for rules of use; OA articles are governed by the applicable Creative Commons License

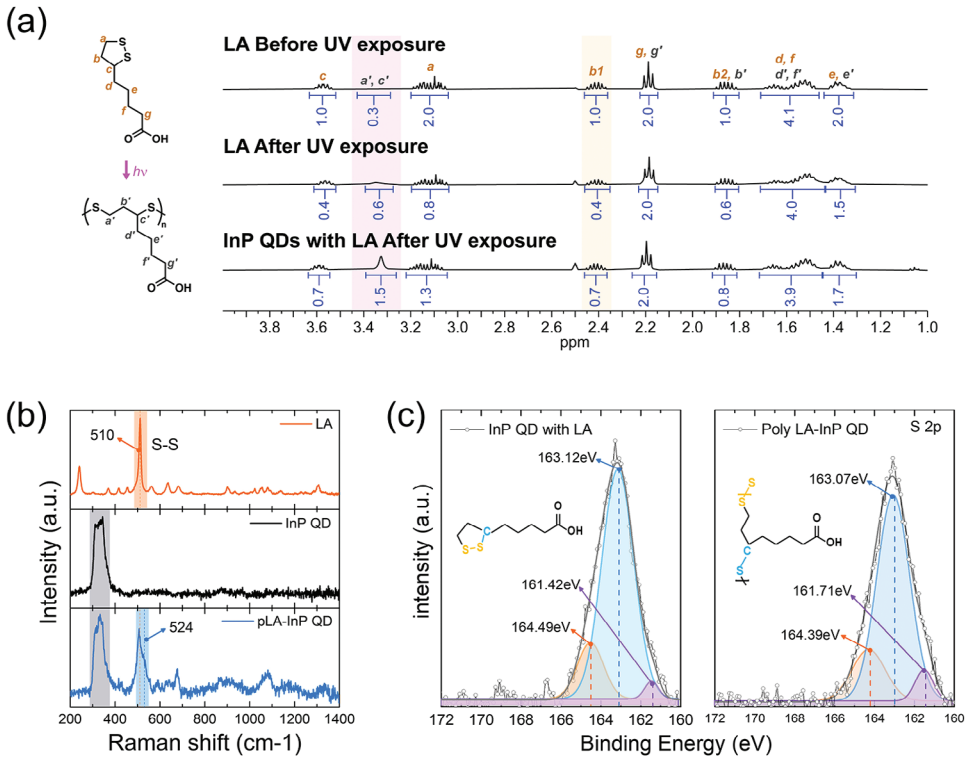

Figure 3. Characteristics of polymerized InP QDs. a) ^{1}H NMR spectra of LA before and after exposure to UV exposure and pLA-InP QD. b) Raman spectra of LA, InP QD, and pLA-InP QD films. c) XPS spectra of LA and pLA-InP QD films. (Note: These XPS samples were prepared using core-only QDs without a sulfide shell to eliminate potential sulfur contributions unrelated to LA.).

protons in the dithiolane ring from the monomer), as detailed in Table S1. While less than 10% of LA self-polymerized in the pristine solution state, UV exposure increased the conversion by almost threefold. With the InP QDs, the conversion efficiency was slightly enhanced, but there was no significant difference in the chemical structure of the pLA.

Raman spectroscopy and XPS were employed to confirm the successful polymerization of LA. The samples for Raman and XPS measurements excluded any influence of sulfur from sources other than LA by using core-only QDs without a shell and partially LA-ligand-exchanged QDs. These core-only QDs also underwent ROP with LA (Figure S9),[39] ensuring that the observed LA polymerization was due to LA ligands and not the shell. As shown in Figure 3b, the sharp peak observed at 510 cm^{-1} in the Raman spectra of LA indicates the presence of a disulfide bond.[40] In the case of pLA-InP QDs, the appearance of two split peaks, including one at 524 cm^{-1}, suggests linear polymerization of LA molecules.[41] This phenomenon likely results from LA reacting and initiating polymerization on the InP QDs. Successful polymerization was confirmed by the presence of these peaks, especially under UV light exposure. According to the XPS results shown in Figure 3c, the S 2p spectrum of both the LA-InP QDs before polymerization and the pLA-InP QDs exposed to UV light exhibited three peaks. The peak around 164 eV corresponds to the S-S bonds in LA's disulfide ring, while the peak around 163 eV is attributed to the C-S bonds in LA. The peak around 161 eV corresponds to bonds formed within the polymer network after LA polymerization.[42,43] The presence of the peak at 161 eV in the LA-InP QDs before polymerization is attributed to in-situ ROP induced by X-ray exposure during XPS measurements and possible ambient light exposure during sample handling. Notably, this peak significantly intensifies after the UV-induced polymerization reaction, confirming the formation of pLA-InP QDs. These results collectively demonstrate that the ROP of LA effectively leads to the formation of a polymerized QD network.

While leveraging the polymerization of disulfide groups in LA significantly enhances the solvent resistance of QD films, UV exposure during this process may potentially degrade the absorption or emission characteristics of QDs, which is undesirable for optoelectronic applications.[44,45] Surprisingly, as shown in **Figure 4a**, the PL intensity of pLA-InP QD films increased sharply after UV exposure, reaching up to 75% higher than that of neat InP QD films. Previous reports on perovskite nanocrystal patterning have noted PL enhancement when short olefin-terminated ligands are used or minor PL increases after crosslinking via thiol-ene click chemistry.[12,46] However, our approach fundamentally differs from these methods.

We investigated the changes in the absorption and emission spectra of the pLA-InP QD films with varying amounts of LA. The absorption curves in Figure 4b show no significant dependence on the LA concentration, whereas the PL intensity exhibits a more complex relationship (Figure S10). The PL intensity increased with the amount of LA, reaching a maximum at 4–6 wt%. Beyond this point, further addition of LA resulted in a diminished increase in PL intensity, suggesting an optimal LA-to-QD ratio,

© 2025 The Author(s). Advanced Materials published by Wiley-VCH GmbH

15214095, 2025, 9, Downloaded from https://advanced.onlinelibrary.wiley.com/doi/10.1002/adma.202415436 by Korea Institute Of Science, Wiley Online Library on [24/07/2025]. See the Terms and Conditions (https://onlinelibrary.wiley.com/terms-and-conditions) on Wiley Online Library for rules of use; OA articles are governed by the applicable Creative Commons License

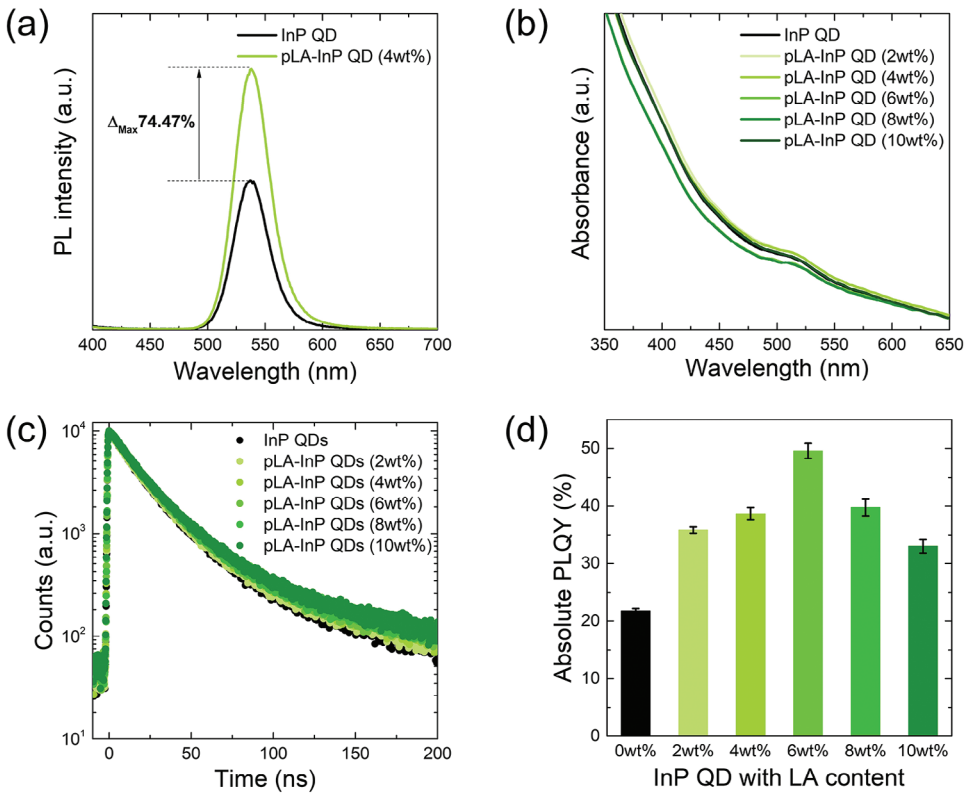

Figure 4. Optical properties of pLA-InP QDs films. a) PL spectra, b) Absorption spectra, c) TRPL decay profiles and (d) Absolute PLQY. (The optical properties of (b), (c) and (d) were measured as a function of the amount of LA.).

with excessive LA negatively impacting the luminescent properties of the composite film. As demonstrated by the TRPL decay curves in Figure 4c, the average decay time (τ_{avg}) increased slightly with higher LA concentrations (Table S2). Notably, the absolute photoluminescence quantum yield (PLQY) measurements shown in Figure 4d reveal that the PLQY peaked at QDs with 6 wt% LA, with a remarkably high value exceeding 50%. However, further increases in LA concentration led to a decrease in PLQY.

This phenomenon can be attributed to the role of LA in passivating surface defects on the QDs. Initially, the LA ligands in the solution contained closed disulfide rings. Upon formation of the QD assembly and subsequent UV exposure, these rings opened, generating thiyl radicals that initiated polymerization. During this process, some thiyl radicals interacted with and passivated defects on the QD surface, thereby enhancing the PL. This mechanism is supported by previous studies demonstrating that organosulfur compounds ligands can enhance the PL of ZnS-coated core-shell QDs.[47,48] As the amount of LA in the solution increased, more defects on the QD shells were likely passivated, leading to the observed increase in absolute PLQY in the film state. Figure 1a also indicates that partial ligand exchange in solution does not immediately enhance the PL. However, the transition to the film state, combined with UV-induced ROP, significantly improved the luminescence properties. This suggests that optimal LA ligand concentrations are critical for protecting and enhancing PL during QD film formation. Similar trends in optical property changes with varying LA content were also observed in the solution state (Figure S11). These results demonstrate that the LA concentration similarly affects QD surface interactions and PL behavior in both film and solution states.

Using optimized conditions, we successfully achieved photo patterns of red, green, and blue QDs, as well as multicolor shapes of various sizes. By selectively exposing the spin-coated LA-QD film on the substrate to i-line UV light (365 nm, 48.6 mW) through photomasks, we developed the desired patterns by spin-coating the LA-QD film and then rinsing it in the QD mother solvent (**Figure 5a**). Figure 5b shows a fluorescence microscopy image of dot patterns with various sizes and spacing at the micrometer scale (first row). We achieved dot patterns as small as 3 μm. The second row of Figure 5b demonstrates that other QD colors, besides green, are feasible. The images depict square patterns of red InP QDs, green InP QDs, and Cd-based blue QDs with 20 μm sizes and 4 μm spacing, corresponding to 1000 pixels per inch (ppi). Each color-specific QD was originally capped with oleic acid, and partial exchange with LA-induced ROP confirmed its capability to achieve the desired color patterns. As mentioned earlier, regardless of the type of native ligand, ROP occurs when the ligands are partially exchanged with LA. Figure S12 further confirms that different native ligands can be used to yield the desired patterns when partially exchanged with LA. Similarly, in the third row of Figure 5b, ring patterns of each color with 10 μm spacing were obtained.

Figure 5c shows fluorescence images of an RGB QD bar pattern array after three photopatterning steps with polymerized LA. The rectangular patterns were 10 μm × 50 μm in size. To obtain an RGB pattern, careful management of the spin coating,

© 2025 The Author(s). Advanced Materials published by Wiley-VCH GmbH

15214095, 2025, 9, Downloaded from https://advanced.onlinelibrary.wiley.com/doi/10.1002/adma.202415436 by Korea Institute Of Science, Wiley Online Library on [24/07/2025]. See the Terms and Conditions (https://onlinelibrary.wiley.com/terms-and-conditions) on Wiley Online Library for rules of use; OA articles are governed by the applicable Creative Commons License

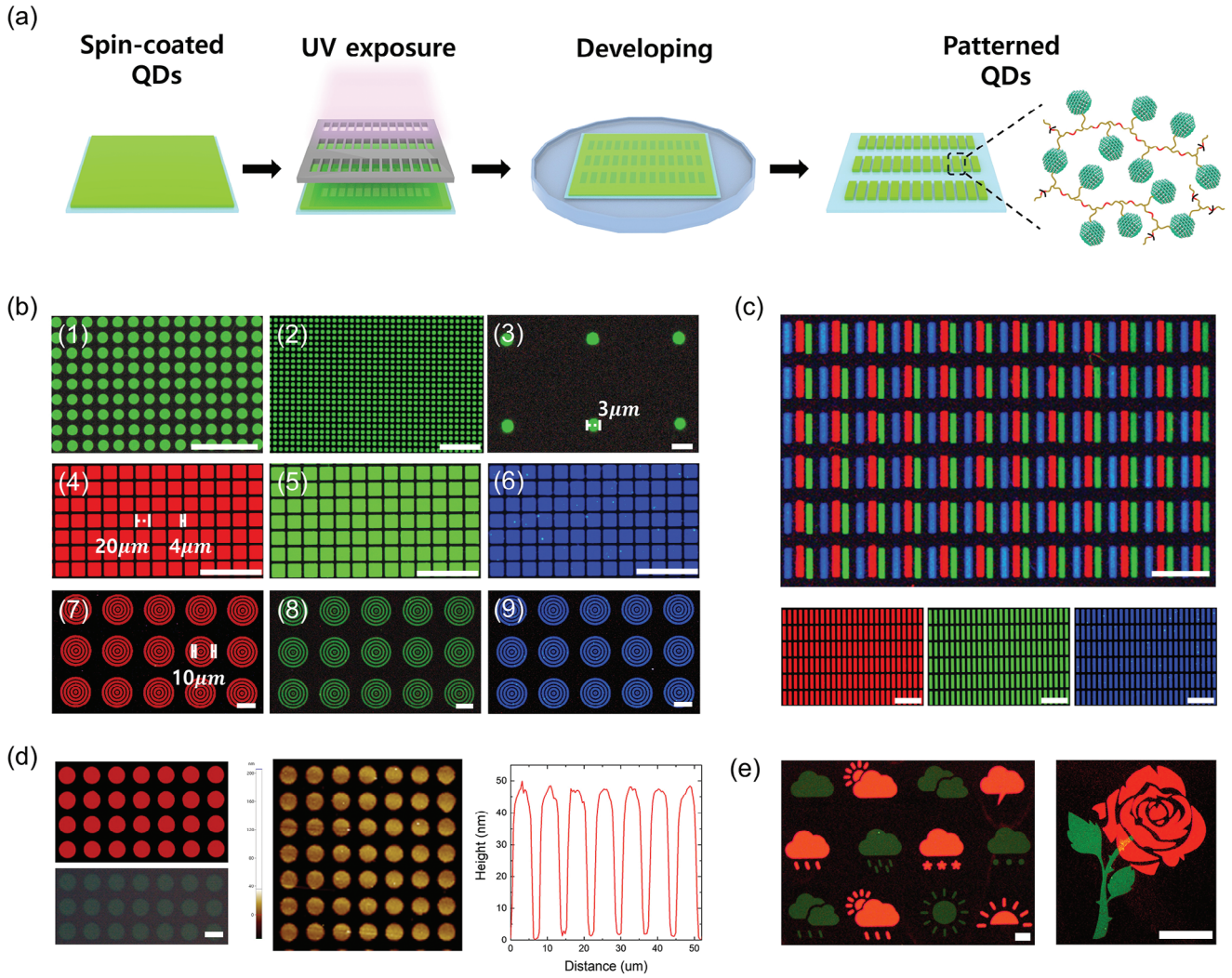

Figure 5. Patterned images of polymerized full-color QDs. a) Schematic of the direct optical patterning process of QDs. b) The first row shows dot patterns with (1) 5 μm size and 2 μm spacing (Scale bar, 100 μm) (1280ppi), (2) 10 μm size and 5 μm spacing (Scale bar, 50 μm) (3386ppi), and (3) 3 μm size (Scale bar, 5 μm) (1571ppi). The second row ((4), (5), and (6)) displays RGB square patterns with 20 μm size and 4 μm spacing (Scale bar, 100 μm) (1000ppi). The last row ((7), (8), and (9)) shows ring patterns with 10 μm spacing (Scale bar, 100 μm) in fluorescence images of pLA-InP QDs patterns. c) Fluorescence images of RGB QD bar patterns with a width of 10 μm and a height of 50 μm (Scale bar, 100 μm) (887ppi). d) Fluorescence, OM, and AFM images with height profiles of dot patterns (Scale bar, 5 μm) (3788ppi). e) Fluorescence images of dual-color pLA-InP QDs with various patterns (Scale bar, 100 μm).

photopatterning, and rinsing processes for differently colored QD films is crucial. When spin-coating QD films of different colors onto previously patterned films, it is essential to prevent contamination or smudging of the underlying layers. Similarly, during rinsing, it is critical to ensure that the underlying layers are not washed away. Achieving precise processing of RGB QDs poses challenges, but Figure 5d shows fluorescence microscopy, optical microscopy (OM), and atomic force microscopy (AFM) images demonstrating well-defined patterns. As shown in the AFM height profile, residues from the mother solvent were removed, leaving only the desired pattern intact. Figure 5d shows patterns of red and green colors in various designs. The distinct visibility of red and green colors individually, as well as the appearance of yellow where red and green overlap, indicates that layers of LA-QDs with different colors can be reliably deposited without damaging the previously coated layers. Fluorescence microscopy images confirm that areas exposed to UV light successfully polymerized the LA ligands, altering the solubility of the QDs in the solvent. This demonstrates the versatility of a simple ligand synthesis process that can be applied to various solution-based applications. Notably, this approach highlights the efficiency of polymerization through the straightforward mechanism of disulfide ring opening and closing.

By introducing additional LA derivatives, we expanded the ROP of LA surface ligands throughout the medium to create stretchable and sustainable QD polymer composites. Octyl lipoamide (OcLAm), synthesized via the carbodiimide coupling reaction of LA with octylamine, was incorporated as a monomer to impart stretchability. Additionally, a suitable amount of 1,2-dithiolane substituted at both ends of bisphenol A (BPA-LA) was

© 2025 The Author(s). Advanced Materials published by Wiley-VCH GmbH

15214095, 2025, 9, Downloaded from https://advanced.onlinelibrary.wiley.com/doi/10.1002/adma.202415436 by Korea Institute Of Science, Wiley Online Library on [24/07/2025]. See the Terms and Conditions (https://onlinelibrary.wiley.com/terms-and-conditions) on Wiley Online Library for rules of use; OA articles are governed by the applicable Creative Commons License

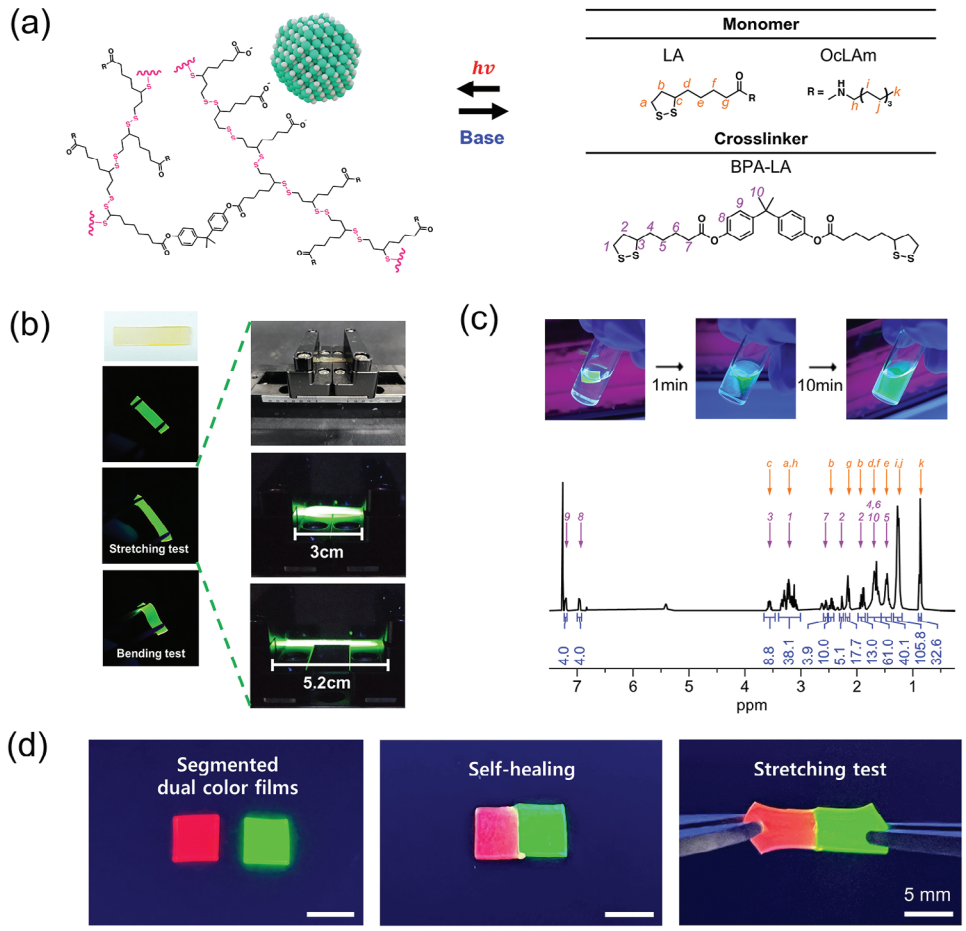

Figure 6. Polymerization and depolymerization of InP QDs polymer film. a) Schematic of polymer film composition containing pLA-InP QDs and composites with attached disulfide ring. b) Photos of the bending test and stretching test of the InP QDs polymer film. c) Photos depicting the depolymerization of InP QDs polymer film through the reversible reaction of disulfide rings and ^{1}H NMR spectra of recovered disulfide monomers. d) Demonstration of self-healing in InP QD polymer films. Red and green InP QD polymer films are joined after base treatment and re-polymerization, indicating the seamless bonding and recovery of the films.

added as a crosslinker to enhance elasticity. Since all polymerizable units consist of 5-membered cyclic disulfides, light or base catalysts can trigger reversible polymerization and depolymerization (**Figure 6**a and S13, Supporting Information).[28] We prepared a mixture of LA-InP QDs, OcLAm, BPA-LA, and 3 mol% Irgacure 819, casting it onto a mold to create crosslinked QD polymer composites after exposure to a white lamp (Figure 6b). The resulting composites were transparent, slightly yellow in color, and exhibited strong green fluorescence under UV light. Furthermore, the elastic polymer matrix enabled flexibility and stretchability (Supplemental Movie). The quasi-static tensile test results revealed that the InP QD polymer film can be stretched up to 178 % with a tensile strength of 176 kPa (Figure S14, Supporting Information).

To address growing concerns about electronic waste, it is essential to design sustainable material systems that can be efficiently recycled through simple processes.[49] LA-based polymers undergo depolymerization by activating open-chain disulfide bonds in dilute solution. We utilized a strong nucleophilic base, 8-diazabicyclo[5.4.0]undec-7-ene (DBU), as the catalyst and immersed a small piece of the composite film in a DBU-containing solution (Figure 6c). Within 10 minutes, the polymer film completely dissolved, indicating a facilitated ring-closing reaction.[50,51] The ^{1}H NMR spectra confirmed the successful recovery of the monomers (OcLAm) and crosslinkers (BPA-LA) to their original forms. Following the depolymerization process, InP QDs were extracted from the mixture, and the recovered QDs exhibited PL spectra identical to those of the pristine QDs (Figure S15). This confirms that the QDs can be effectively recycled through depolymerization. The polymerization and depolymerization reactions of the LA-based QD composites present significant findings for both science and industry, indicating that QDs can be used in multi-form-factor applications and are recyclable.

The facile opening and closing of the disulfide ring (1,2-dithiolane) during polymerization and depolymerization, along with the self-healing process, is illustrated in Figure 6d.[28,50,51] To demonstrate self-healing capability of our polymers, we prepared two differently colored InP QD films (red and green) using OcLAm as monomers, BPA-LA as crosslinkers, and Irgacure 819 as initiators. Each film was cut in half with a knife and the cut edges were placed in direct contact for 30 minutes at

© 2025 The Author(s). Advanced Materials published by Wiley-VCH GmbH

15214095, 2025, 9, Downloaded from https://advanced.onlinelibrary.wiley.com/doi/10.1002/adma.202415436 by Korea Institute Of Science, Wiley Online Library on [24/07/2025]. See the Terms and Conditions (https://onlinelibrary.wiley.com/terms-and-conditions) on Wiley Online Library for rules of use; OA articles are governed by the applicable Creative Commons License

15214095, 2025, 9, Downloaded from https://advanced.onlinelibrary.wiley.com/doi/10.1002/adma.202415436 by Korea Institute Of Science, Wiley Online Library on [24/07/2025]. See the Terms and Conditions (https://onlinelibrary.wiley.com/terms-and-conditions) on Wiley Online Library for rules of use; OA articles are governed by the applicable Creative Commons License

room temperature after applying a DBU solution. A strong base like DBU is known to accelerate disulfide exchange reactions, enabling self-healing under ambient conditions. Following this process, the two differently colored polymer films seamlessly merged into a single film. Furthermore, the resulting dual-color film exhibited excellent stretchability, confirming that the self-healing process fully restored its structural and functional integrity. This process demonstrates that the composite films, made stretchable and reversible through ROP, hold promise for various applications in display technology and can be further expanded in their potential uses.

3. Conclusion

This study presents a novel approach for direct optical patterning of QD assemblies using LA as a polymerizable ligand. By leveraging the ROP of LA under UV exposure, we successfully enhanced the solvent resistance and PL stability of QD films. This method enables the creation of high-resolution RGB patterns, demonstrating its applicability in advanced microdisplays. Furthermore, the incorporation of LA-derived monomers facilitates the fabrication of stretchable and self-healing QD composites, addressing the growing demand for flexible and sustainable materials in modern display technologies. The reversible ROP process also supports the recovery and recycling of QDs, contributing to environmental sustainability. Our findings suggest that LA-based QD assemblies not only improve traditional QD patterning techniques but also open new avenues for their application in emerging technologies, such as AR/VR displays and wearable electronics. This study highlights the potential of LA-based strategies to significantly impact the development of next-generation optoelectronic devices, offering a versatile and durable platform for future innovations.

4. Experimental Section

Materials: (±)-α-LA (ACS reagent, ≥98.0%) was sourced from Sigma-Aldrich. Indium acetate ($In(OAc)_3$), zinc acetate ($Zn(OAc)_2$), selenium, sulfur, 1-octadecene (ODE, 90%), oleic acid (OA, 90%), trioctylphosphine (TOP, 97%), and toluene (anhydrous 99.8%) were obtained from Sigma–Aldrich. Tris(trimethylsilyl)phosphine (TMS_3P) was acquired from SK Chemicals. DL-α-LA, ≥99%) and 1-(3-dimethylaminopropyl)-3-ethylcarbodiimide hydrochloride (EDCI, ≥98%) were purchased from TCI Chemicals. 4-(Dimethylamino) pyridine (DMAP, ≥99%), octylamine (99%), phenylbis(2,4,6-trimethylbenzoyl) phosphine oxide (Irgacure 819, 97%), and bisphenol A (BPA, ≥99%) were sourced from Sigma-Aldrich. Dichloromethane (DCM, 99.7%) was obtained from Alfa Chemicals, and acetonitrile (MeCN, 99.9%) was acquired from Daejung Chemistry.

Synthesis of InP QDs: The green-emitting InP core was synthesized under a nitrogen atmosphere using the Schlenk line technique. In a 50 mL three-neck flask, 1.2 mmol of $In(OAc)_3$, 0.6 mmol of $Zn(OAc)_2$, and 4.8 mmol of ODE (10 mL) were combined and degassed under vacuum at 105 °C for 2 hours. The reaction flask was then heated to 240 °C for 1.5 hours to form In/Zn oleate, which was subsequently cooled to 120 °C. A 0.2 M solution of TMS_3P/TOP (4 mL) was rapidly injected into the flask, which was heated to 260 °C for 30 minutes to grow the InP cores. Afterward, a 0.5 M ZnOA solution (2 mL) and a 1 M TOP

Solution (1 mL) were sequentially injected, and the reaction was held at 260 °C for 30 minutes before cooling to room temperature. The mixture was transferred to an N_2-filled glove box and purified twice using toluene and ethanol. The InP cores were diluted in 8 mL of toluene and stored in the glove box until needed. For shell growth, a solution of 2 mmol $Zn(OAc)_2$, 4 mmol OA, and 10 mL ODE was degassed at 105 °C for 1 hour, followed by refilling with N_2. The mixture was then heated to 250 °C for 30 minutes to form a ZnOA solution and cooled to 80 °C. The InP core solution (1 mL) was injected into the flask, and the solvent was evaporated under vacuum. After refilling with N_2, the solution was heated to 200 °C for 5 minutes, followed by the rapid injection of 0.3 mL TOP and heating to 280 °C for 30 minutes. A 0.3 mL solution of TOP was subsequently added, and the mixture was heated to 300 °C for 1 hour to grow the ZnS shell. The flask was cooled to room temperature, and the resultant InP QDs were purified using toluene and ethanol and diluted in toluene for future use.

Direct Patterning Process: Si or SiO_2 substrates were cleaned using ultrasonication in acetone and isopropanol for 15 minutes each, followed by drying to remove solvents completely. The substrates were treated with UV-ozone for 15 minutes. To exchange QD ligands partially, a solution of LA (30 mg/mL) in toluene was mixed with a 6 wt% solution of QDs in toluene (30 mg/mL). The ligand-exchanged QDs were spin-coated onto the substrate at 2000 rpm for 30 seconds using a 0.45 μm PTFE filter to avoid aggregation. A photomask was aligned onto the QD-coated substrate using a mask aligner (Mask Aligner MDA-400M, Midas System). UV light (≈ 40 mW/cm^2) was applied for 2 minutes and 30 seconds. The substrate was then immersed in toluene for 1 minute and 30 seconds to develop the unexposed regions, and residual solvent was removed by air blowing. The same process was applied to create multiple patterns using different types of QDs.

Synthesis of LA-Modified Bifunctional Crosslinker (BPA-LA): BPA (0.5 g, 2.19 mmol, 1 equiv.), EDCI (1.85 g, 9.65 mmol, 2.2 equiv.), and DMAP (0.11 g, 0.90 mmol, 0.2 equiv.) were added to a round-bottom flask, which was purged with Ar. MeCN (30 mL) was then introduced, and the mixture was stirred for 5 minutes. LA (1.13 g, 5.48 mmol, 2.5 equiv.) in MeCN (10 mL) was added and stirred for 24 hours at room temperature. The solvent was removed, and the product was purified by column chromatography to yield light yellow powders (1.22 g, 2.01 mmol, 92%).

^{1}H NMR (400 MHz, $CDCl_3$) δ 7.27 – 7.20 (m, 2H), 7.04 – 6.95 (m, 2H), 3.62 (dq, J = 8.5, 6.4 Hz, 1H), 3.26 – 3.11 (m, 2H), 2.59 (t, J = 7.4 Hz, 2H), 2.55 – 2.43 (m, 1H), 2.02 – 1.88 (m, 1H), 1.79 (dddd, J = 23.8, 14.2, 7.8, 4.5 Hz, 4H), 1.69 (s, 3H), 1.58 (tqd, J = 18.2, 6.1, 2.0 Hz, 2H).^{13}C NMR (101 MHz, $CDCl_3$) δ 172.11, 148.64, 147.90, 127.90, 120.99, 56.39, 42.55, 40.31, 38.60, 34.69, 34.23, 31.03, 28.79, 24.75.

Synthesis of 5-(1,2-dithiolan-3-yl)-N-Octylpentanamide (Octyl Lipoamide, OcLAm): EDCI (3.07 g, 15.9 mmol, 1.1 equiv.) and DMAP (0.18 g, 0.15 mmol, 0.1 equiv.) were placed in a round-bottom flask, purged with Ar, and DCM (60 mL) was added. Octylamine (3.6 mL, 21.8 mmol, 1.5 equiv.) was added once the solution became clear, followed by LA (3.00 g, 14.5 mmol, 1.0 equiv.) in DCM (30 mL), and the mixture was stirred for 24 hours at room temperature. The product was condensed and purified by column chromatography to yield yellowish solids (4.24 g, 13.3 mmol, 92%).

^{1}H NMR (400 MHz, $CDCl_3$) δ 5.69 (s, 1H), 3.60 (p, J = 6.5 Hz, 1H), 3.34 – 3.07 (m, 4H), 2.49 (dq, J = 12.5, 6.2 Hz, 1H), 2.29 – 2.17 (m, 2H), 1.94 (dq, J = 13.5, 6.9 Hz, 1H), 1.72 (dp, J = 17.3, 7.6 Hz, 4H), 1.50 (tq, J = 12.1, 6.7 Hz, 4H), 1.39 – 1.19 (m, 10H), 0.90 (t, J = 6.6 Hz, 3H).

^{13}C NMR (101 MHz, $CDCl_3$) δ 172.70, 56.51, 40.31, 39.62, 38.54, 36.60, 34.71, 31.86, 29.74, 29.34, 29.28, 28.98, 27.02, 25.56, 22.71, 14.17.

Synthesis of InP QD Polymer Film: A polymerization reaction was conducted in a custom glass mold, with a silicone spacer sandwiched between two glass sheets. These were treated with vaporized perfluorodecyltriethoxysilane to facilitate detachment. Irgacure 819 (9.9 mg, 0.023 mmol, 1 equiv.), octyl lipoamide (250 mg, 0.79 mmol, 33 equiv.), and BPA-LA (47.6 mg, 0.079 mmol, 3.3 equiv.) were placed in vials, purged, and filled with Ar. Chlorobenzene (0.5 mL) was added and stirred, followed by the addition of an InP solution (0.16 mL, 1 wt%). The mixture was injected into a mold, the solvent was evaporated in a vacuum oven, and the mixture was photo-cured with a white lamp (≈ 70 mW/cm^2) for 1 hour, producing a yellowish film.

Characterization: TEM images were acquired using a JEOL JEM-2010 instrument at 200 kV. UV-visible absorption spectra were measured using a Shimadzu UV-2600 spectrometer, and PL spectra were recorded

© 2025 The Author(s). Advanced Materials published by Wiley-VCH GmbH

on a Horiba Fluoromax-4 at 375 nm excitation and 0.5 nm resolution. PLQYs were obtained with an integrating sphere. Time-resolved PL decays were measured using a Horiba DeltaDiode-375L pulsed laser diode ($\lambda = 375$ nm) and a time-correlated single-photon counting module. Zeta potential analysis was performed on a Zetasizer Nano ZS (Malvern). ^{1}H NMR spectra were measured using a Bruker Avance III 400 MHz with $CDCl_3$ and DMSO as solvents. Raman spectroscopy was performed using LabRAM Aramis (Horiba Jobin Yvon) with a 785 nm laser. XPS was carried out on a Thermo Electron K-alpha spectrometer. Patterned images were obtained using the Mask Aligner MDA-400M, and fluorescence images were acquired using an Olympus BX51 microscope with a DP74 camera. OM images were captured on an Olympus BX51 microscope. AFM measurements were performed on an NX20 (Park Systems). GISAXS measurements were conducted on an XENOCS XEUSS 2.0, and MALDI-TOF measurements were obtained using a Shimadzu Biotech AXIMA with a DHB matrix. Stress-strain tests were measured by using Dynamic Mechanical Analysis (DMA) (Q 800, TA Instruments).

Supporting Information

Supporting Information is available from the Wiley Online Library or from the author.

Acknowledgements

Y.L., S.J., and S.S. contributed equally to this work. N.O. acknowledges financial support from the National Research Foundation (NRF) of Korea and grants were funded by the Ministry of Science, ICT (grant numbers: 2022M3H4A1A03076093, RS-2024-00411892, and RS-2024-00358337). T.A. Kim acknowledges the financial support from a National Research Council of Science & Technology (NST) grant from the Korean government (MSIT) (CRC22031-000).

Conflict of Interest

The authors declare no conflict of interest.

Data Availability Statement

The data that support the findings of this study are available from the corresponding author upon reasonable request.

Keywords

direct optical lithography, polymerization, QD nanocomposites, quantum dots

Received: October 10, 2024
Revised: December 6, 2024
Published online: January 13, 2025

[1] S. Kim, K. Lee, N. Gwak, S. Shin, J. Seo, S. H. Noh, D. Kim, Y. Lee, H. Kong, D. Yeo, S. Y. Lee, J. Jang, N. Oh, *Adv. Mater.* **2024**, *36*, 2310671.
[2] S. Shin, N. Gwak, H. Yoo, H. Jang, M. Lee, K. Kang, S. Kim, S. Yeon, T. Ann Kim, S. Kim, G. W. Hwang, N. Oh, *Chem. Eng. J.* **2023**, *466*, 143223.
[3] D. V. Talapin, J. S. Lee, M. V. Kovalenko, E. V. Shevchenko, *Chem. Rev.* **2010**, *110*, 389.
[4] L. A. Kim, P. O. Anikeeva, S. A. Coe-Sullivan, J. S. Steckel, M. G. Bawendi, V. Bulović, *Nano Lett.* **2008**, *8*, 4513.
[5] M. K. Choi, J. Yang, K. Kang, D. C. Kim, C. Choi, C. Park, S. J. Kim, S. I. Chae, T. H. Kim, J. H. Kim, T. Hyeon, D. H. Kim, *Nat. Commun.* **2015**, *6*, 7149.
[6] J. Yoo, K. Lee, U. J. Yang, H. H. Song, J. H. Jang, G. H. Lee, M. S. Bootharaju, J. H. Kim, K. Kim, S. I. Park, J. D. Seo, S. Li, W. S. Yu, J. I. Kwon, M. H. Song, T. Hyeon, J. Yang, *Nat. Photonics* **2024**, *18*, 1105.
[7] Y. Liu, F. Li, Z. Xu, C. Zheng, T. Guo, X. Xie, L. Qian, D. Fu, X. Yan, *ACS Appl. Mater. Interfaces* **2017**, *9*, 25506.
[8] S. Jia, H. Tang, J. Ma, S. Ding, X. Qu, B. Xu, Z. Wu, G. Li, P. Liu, K. Wang, X. W. Sun, *Adv. Opt. Mater.* **2021**, *9*, 2101069.
[9] D. Hahm, J. Lim, H. Kim, J. W. Shin, S. Hwang, S. Rhee, J. H. Chang, J. Yang, C. H. Lim, H. Jo, B. Choi, N. S. Cho, Y. S. Park, D. C. Lee, E. Hwang, S. Chung, C. mo Kang, M. S. Kang, W. K. Bae, *Nat. Nanotechnol.* **2022**, *17*, 952.
[10] J. Yang, D. Hahm, K. Kim, S. Rhee, M. Lee, S. Kim, J. H. Chang, H. W. Park, J. Lim, M. Lee, H. Kim, J. Bang, H. Ahn, J. H. Cho, J. Kwak, B. S. Kim, C. Lee, W. K. Bae, M. S. Kang, *Nat. Commun.* **2020**, *11*, 2874.
[11] S. Shin, Y. Kim, N. Gwak, I. Jeong, M. Lee, K. Kang:, S. Yeon, S. Kim, T. A. Kim, *N. Oh, Appl. Surf. Sci.* **2023**, *608*, 155016.
[12] S. Shin, K. Kang, H. Jang, N. Gwak, S. Kim, T. A. Kim, N. Oh, *Small Methods* **2023**, *7*, 2300206.
[13] W. Mei, Z. Zhang, A. Zhang, D. Li, X. Zhang, H. Wang, Z. Chen, Y. Li, X. Li, X. Xu, *Nano Res.* **2020**, *13*, 2485.
[14] J. S. Park, J. Kyhm, H. H. Kim, S. Jeong, J. Kang, S. E. Lee, K. T. Lee, K. Park, N. Barange, J. Han, J. D. Song, W. K. Choi, I. K. Han, *Nano Lett.* **2016**, *16*, 6946.
[15] J. A. Pan, H. Cho, I. Coropceanu, H. Wu, D. V. Talapin, *Acc. Chem. Res.* **2023**, *56*, 2286.
[16] J. Lee, J. Ha, H. Lee, H. Cho, D. C. Lee, D. V. Talapin, H. Cho, *ACS Energy Lett.* **2023**, *8*, 4210.
[17] P. Xiao, Z. Zhang, J. Ge, Y. Deng, X. Chen, J. R. Zhang, Z. Deng, Y. Kambe, D. V. Talapin, Y. Wang, *Nat. Commun.* **2023**, *14*, 49.
[18] J. A. Pan, Z. Rong, Y. Wang, H. Cho, I. Coropceanu, H. Wu, D. V. Talapin, *J. Am. Chem. Soc.* **2021**, *143*, 2372.
[19] Y. Wang, X. Shan, Y. Tang, T. Liu, B. Li, P. Jin, K. Liang, D. Li, Y. M. Yang, H. Shen, B. Zhu, B. Ji, A. C. S. Appl, *Nano Mater* **2022**, *5*, 8457.
[20] J. A. Pan, J. C. Ondry, D. V. Talapin, *Nano Lett.* **2021**, *21*, 7609.
[21] H. T. Zhang, L. K. Hou, G. W. Chu, J. X. Wang, L. L. Zhang, J. F. Chen, *Chem. Eng. J.* **2024**, *482*, 148816.
[22] Q. Zhang, D. H. Qu, B. L. Feringa, H. Tian, *J. Am. Chem. Soc.* **2022**, *144*, 2022.
[23] C. Cai, S. Wu, Y. Zhang, F. Li, Z. Tan, S. Dong, *Adv. Sci.* **2022**, *9*, 2203630.
[24] H. Mattoussi, J. M. Mauro, E. R. Goldman, G. P. Anderson, V. C. Sundar, F. V. Mikulec, M. G. Bawendi, *J. Am. Chem. Soc.* **2000**, *122*, 12142.
[25] K. Susumu, B. C. Mei, H. Mattoussi, *Nat. Protoc.* **2009**, *4*, 424.
[26] N. Zhan, G. Palui, H. Mattoussi, *Nat. Protoc.* **2015**, *10*, 859.
[27] M. La Rosa, T. Avellini, C. Lincheneau, S. Silvi, I. A. Wright, E. C. Constable, A. Credi, *Eur. J. Inorg. Chem.* **2017**, *2017*, 5143.
[28] J. Lee, G. Park, D. Lee, J. Shin, C. Ahn, J. Lee, T. A. Kim, *Mater. Horizons* **2024**, *11*, 5220.
[29] M. K. Choi, J. Yang, T. Hyeon, D. H. Kim, *Electron* **2018**, *2*, 10.
[30] J. Ko, B. G. Jeong, J. H. Chang, J. F. Joung, S. Y. Yoon, D. C. Lee, S. Park, J. Huh, H. Yang, W. K. Bae, S. G. Jang, J. Bang, *NPG Asia Mater* **2020**, *12*, 19.
[31] W. Wang, A. Kapur, X. Ji, M. Safi, G. Palui, V. Palomo, P. E. Dawson, H. Mattoussi, *J. Am. Chem. Soc.* **2015**, *137*, 5438.
[32] M. J. Choi, F. P. García de Arquer, A. H. Proppe, A. Seifitokaldani, J. Choi, J. Kim, S. W. Baek, M. Liu, B. Sun, M. Biondi, B. Scheffel, G. Walters, D. H. Nam, J. W. Jo, O. Ouellette, O. Voznyy, S. Hoogland,

© 2025 The Author(s). Advanced Materials published by Wiley-VCH GmbH

15214095, 2025, 9, Downloaded from https://advanced.onlinelibrary.wiley.com/doi/10.1002/adma.202415436 by Korea Institute Of Science, Wiley Online Library on [24/07/2025]. See the Terms and Conditions (https://onlinelibrary.wiley.com/terms-and-conditions) on Wiley Online Library for rules of use; OA articles are governed by the applicable Creative Commons License

S. O. Kelley, Y. S. Jung, E. H. Sargent, *Nat. Commun.* **2020**, *11*, 103.
[33] M. C. Weidman, K. G. Yager, W. A. Tisdale, *Chem. Mater.* **2015**, *27*, 474.
[34] W. Fang, Z. Mu, Y. He, K. Kong, K. Jiang, R. Tang, Z. Liu, *Nature* **2023**, *619*, 293.
[35] E. Jang, Y. Kim, Y. H. Won, H. Jang, S. M. Choi, *ACS Energy Lett.* **2020**, *5*, 1316.
[36] N. Reitinger, A. Hohenau, S. Köstler, J. R. Krenn, A. Leitner, *Phys. Status Solidi Appl. Mater. Sci.* **2011**, *208*, 710.
[37] A. Radchanka, V. Hrybouskaya, A. Iodchik, A. W. Achtstein, M. Artemyev, *J. Phys. Chem. Lett.* **2022**, *13*, 4912.
[38] B. Fritzinger, R. K. Capek, K. Lambert, J. C. Martins, Z. Hens, *J. Am. Chem. Soc.* **2010**, *132*, 10195.
[39] N. Gwak, S. Shin, H. Yoo, G. W. Seo, S. Kim, H. Jang, M. Lee, T. H. Park, B. J. Kim, J. Lim, S. Y. Kim, S. Kim, G. W. Hwang, N. Oh, *Adv. Mater.* **2024**, *36*, 2404480.
[40] B. Hernández, F. Pflüger, E. López-Tobar, S. G. Kruglik, J. V. Garcia-Ramos, S. Sanchez-Cortes, M. Ghomi, *J. Raman Spectrosc.* **2014**, *45*, 657.
[41] C. Dang, M. Wang, J. Yu, Y. Chen, S. Zhou, X. Feng, D. Liu, H. Qi, *Adv. Funct. Mater.* **2019**, *29*, 1902467.
[42] L. Kong, Y. Yang, M. Wu, X. Teng, Y. Wang, C. Xu, *Int. J. Biol. Macromol.* **2022**, *223*, 446.
[43] C. Chen, X. Yang, S. J. Li, C. Zhang, Y. N. Ma, Y. X. Ma, P. Gao, S. Z. Gao, X. J. Huang, *Green Chem.* **2021**, *23*, 1794.
[44] S. Jun, J. Lee, E. Jang, *ACS Nano* **2013**, *7*, 1472.
[45] J. Lim, W. K. Bae, D. Lee, M. K. Nam, J. Jung, C. Lee, K. Char, S. Lee, *Chem. Mater.* **2011**, *23*, 4459.
[46] M. J. Smith, S. T. Malak, J. Jung, Y. J. Yoon, C. H. Lin, S. Kim, K. M. Lee, R. Ma, T. J. White, T. J. Bunning, Z. Lin, V. V. Tsukruk, *ACS Appl. Mater. Interfaces* **2017**, *9*, 17435.
[47] G. Almeida, L. van der Poll, W. H. Evers, E. Szoboszlai, S. J. W. Vonk, F. T. Rabouw, A. J. Houtepen, *Nano Lett.* **2023**, *23*, 8697.
[48] J. W. Trzciński, L. Morillas-Becerril, S. Scarpa, M. Tannorella, F. Muraca, F. Rastrelli, C. Castellani, M. Fedrigo, A. Angelini, R. Tavano, E. Papini, F. Mancin, *Biomacromolecules* **2021**, *22*, 467.
[49] J. Lee, D. Lee, C. H. Ahn, T. A. Kim, *Adv. Funct. Mater.* **2024**, 2414842.
[50] X. Zhang, R. M. Waymouth, *J. Am. Chem. Soc.* **2017**, *139*, 3822.
[51] B. Wang, Q. Zhang, Z. Wang, C. Shi, X. Gong, H. Tian, D. Qu, *Angew. Chemie* **2023**, *62*, 202215329.

© 2025 The Author(s). Advanced Materials published by Wiley-VCH GmbH

15214095, 2025, 9, Downloaded from https://advanced.onlinelibrary.wiley.com/doi/10.1002/adma.202415436 by Korea Institute Of Science, Wiley Online Library on [24/07/2025]. See the Terms and Conditions (https://onlinelibrary.wiley.com/terms-and-conditions) on Wiley Online Library for rules of use; OA articles are governed by the applicable Creative Commons License